Sādhanā Vol. 28, Parts 3 & 4, June/August 2003, pp. 677–693. © Printed in India

Toughening and creep in multiphase intermetallics through microstructural control

A K GOGIA, R G BALIGIDAD and D BANERJEE

Defence Metallurgical Research Laboratory, Hyderabad 500 258, India

Abstract. The lack of engineering ductility in intermetallics has limited their structural applications, in spite of their attractive specific properties at high temperatures. Over the last decade, research in intermetallics has been stimulated by the discovery of remarkable ductilisation mechanisms in these materials. It has however often been the case that the process of ductilisation or toughening has also led to a decrease in high temperature properties, especially creep. In this paper we describe approaches to the ductilisation of two different classes of intermetallic alloys through alloying to introduce beneficial, second phase effects. The Ti_2AlNb based intermetallics in the Ti–Al–Nb system can be ductilised by stabilising the *bcc* phase of titanium into the structure. The principles of microstructural and compositional optimization developed to achieve adequate plasticity, while retaining creep properties of these alloys, are described. An entirely different approach has been successful in imparting plasticity to intermetallics based on Fe_3Al. The addition of carbon to form the $Fe_3AlC_{0\cdot5}$ phase imparts ductility, while enhancing both tensile and creep strength.

Keywords. Multiphase intermetallics; multistructural control; toughening; creep.

1. Introduction

Intensive research over the last two decades has led to the emergence of intermetallics as a new class of engineering materials that provide enhanced combinations of low density, stiffness, creep and high temperature strength as primary properties, and optimized and acceptable levels of ductility, toughness, fatigue resistance and environmental resistance required for a variety of applications. Ductility and toughness are key requirements in structural use. It is however quite clear from the intensive research in this area that acceptable ductility and toughness are most often obtained at the expense of high temperature properties such as creep. A fundamental reason for this appears to be that the very factors that lead to low plasticity in intermetallics, that is anisotropy of charge density in the crystal structure or directionality of bonding, also provide enhanced high temperature properties.

In this paper, we describe our recent research exploring these issues in two intermetallic systems, the first based on the Ti_2AlNb phase and the second on the Fe_3Al phase. Alloying these intermetallics to introduce additional phases enhances the spectrum of microstructural options that can be directed towards obtaining acceptable combinations of ductility, toughness and

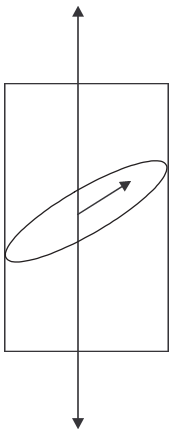

Figure 1. Single crystal behaviour, σ cleavage is reached before $\tau_{app} = \tau_{crss}$.

high temperature mechanical properties. This description is preceded by a brief background on plasticity in intermetallics.

2. Ductilisation of intermetallics

Engineering plasticity is required in structural materials to redistribute stress concentrations that might exist locally at macrodefects which are always assumed to exist in any structural component. Plasticity is governed by dislocation generation and mobility in a single crystal of the material, and single crystals may be said to brittle if at any temperature or strain rate, the cleavage stress is reached before resolved shear stress due to an applied monotonic tensile stress exceeds the critical resolved shear stress for slip on a favourably oriented slip system (figure 1). Thus, plasticity in single crystals can depend strongly on the orientation of the load axis with respect to the crystal orientation. Additional constraints emerge in a polycrystalline assemblage, since five independent slip systems are required to accommodate a general shape change in a polycrystalline assemblage. A simple criterion for plasticity in a polycrystalline system is provided in the relationships given in figure 2. These provide a physical basis for enhancing plasticity in polycrystalline system. Figure 3 expresses the same viewpoint in an alternative manner. If the relative values of applied stress, yield stress, and fracture stresses are close to one another in magnitude, the stress concentration at the grain boundary can result in a local stress that can induce yield or fracture depending upon the relative value of these stresses. Thus, plasticity or brittle behaviour in many intermetallics can be affected by small changes in the relative values of these stresses and their dependence on strain rate or temperature, as well as the work-hardening rate.

Figure 4 provides two examples of the effect of changing the Taylor orientation factor by increasing the number of slip systems. In the Ni_3V case the effect is related to changing the crystal structure to one of higher symmetry, while in the BCC example, the operative slip system depends on the antiphase boundary energy associated with the $\frac{1}{2}\langle 111\rangle$ Burgers vector. If the APB energy is high then the $\langle 100\rangle$ slip is preferred, and is associated with brittle behaviour, as in polycrystalline NiAl. However, polycrystalline Fe_3Al is brittle even though the operative slip system is $\langle 111\rangle$; obviously a relatively low cleavage stress dominates properties. The low cleavage stress is believed to arise from dynamic effects arising from hydrogen interaction with the material during tensile testing as can be deduced from the

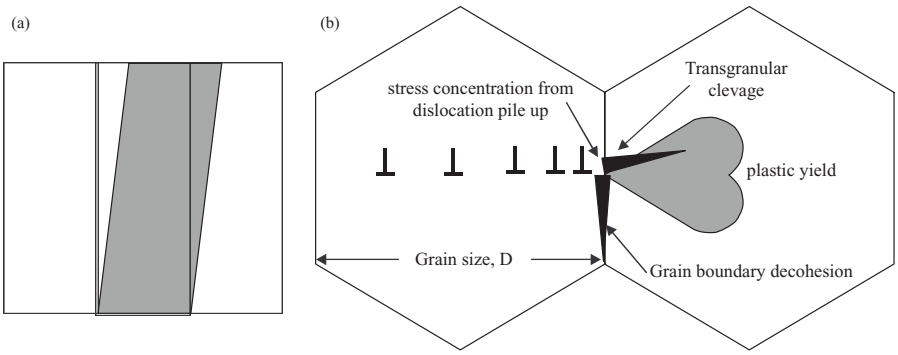

Figure 2. The criteria for ductility in polycrystalline materials. **(a)** Polycrystal brittle – 5 independent slip systems for general shape change. **(b)** Fracture occurs when $\sigma_\varepsilon D^{1/2} k_\varepsilon > \beta G\gamma$. $k_\varepsilon = m^2 \tau_I r^{1/2} + Am^{3/2}\varepsilon^{1/2}$. Decrease – σ_ε: single crystal flow stress; m: Taylor orientation factor; τ_i: slip transfer stress; D: grain size. Increase – γ: surface energy for cleavage or grain boundary decohesion stress.

properties shown in table 1 when Fe_3Al is tested in different environments. Ni_3Al is an example of a material that is ductile in single crystal form, but brittle in polycrystalline form, is Ni_3Al. The low polycrystalline ductility of Ni_3Al is attributed to its intrinsically low grain boundary strength as discussed previously, and the effect of boron on enhancing the ductility of substoichiometric Ni_3Al through its strengthening effect on grain boundaries is one of the classic stories of intermetallic research.

3. Intermetallics based on the Ti_2AlNb system

3.1 *Background*

Alloys based on the intermetallic Ti_3Al have been investigated since the sixties (McAndrew & Simcoe 1961) towards obtaining high temperature titanium-based materials that can replace

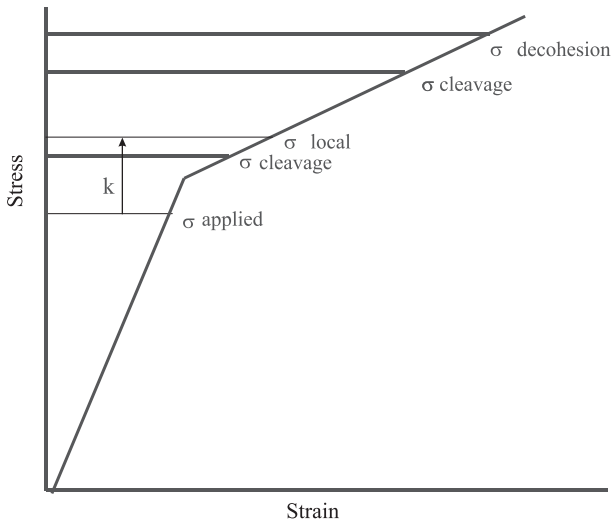

Figure 3. The ductility in polycrystalline materials is controlled by the local stress at grain boundaries in relation to the fracture stress terms.

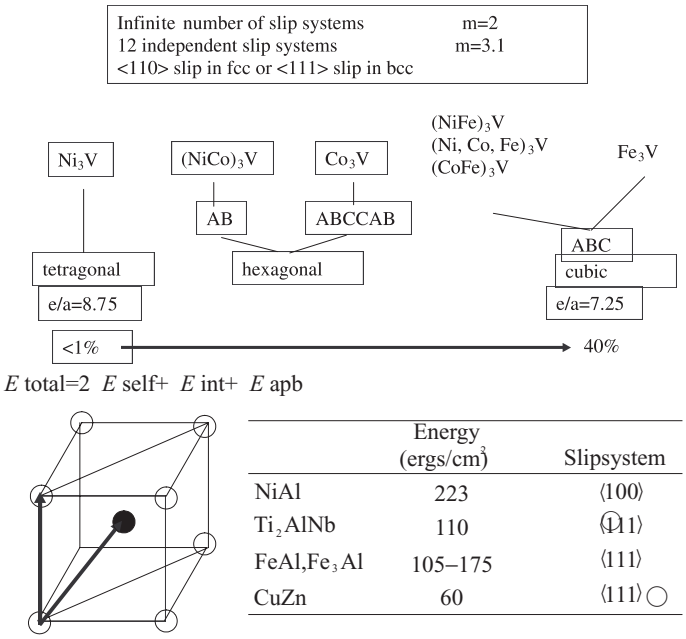

	Energy (ergs/cm^2)	Slipsystem
NiAl	223	⟨100⟩
Ti_2AlNb	110	⟨111⟩
FeAl,Fe_3Al	105–175	⟨111⟩
CuZn	60	⟨111⟩

Figure 4. The influence of crystal structure and APB energy on the operative slip system.

heavier Ni-base alloys in the temperature range 550°–750°C. It was demonstrated in the early seventies (Blackburn & Smith 1978) that plasticity could be obtained in this system through Nb additions at a level adequate to stabilize the high temperature *bcc* allotrope of Ti into the structure. The *bcc* phase was found to be present in its ordered form, the B2 phase. In the eighties (Rowe 1991), improved combinations of ductility, strength and creep (figures 5 and 6) were obtained through enhanced Nb additions, as a result of two principal effects. The first was the modification of the Ti_3Al phase to a ternary intermetallic, the Ti_2AlNb phase (Banerjee *et al* 1988) (distorted from the *hcp* structure of Ti_3Al to an orthorhombic symmetry). The second emerged as a consequence of slower reaction kinetics of diffusion-driven microstructural changes in the high Nb alloys, resulting in finer scales of microstructure in the multi-phase system. The physical metallurgy of this system was understood in greater detail in the nineties (Banerjee *et al* 1993; Banerjee 1994; Banerjee 1997; Gogia *et al* 1998). We describe in the following sections this understanding with respect to strength, ductility,

Table 1. The effect of test environment on the ductility of Fe_3Al.

Transgranular ⟶ Intergranular

	Property	Air	Oxygen
Fe_3Al	El(%)	4·0	12
	YS(MPa)	387	392
	YTS(MPa)	559	867
Fe-36Al	El(%)	2	11·3
	YS(MPa)	360	373
	YTS(MPa)	412	677
Fe_3Al + Cr + Nb	El(%)	> 15	

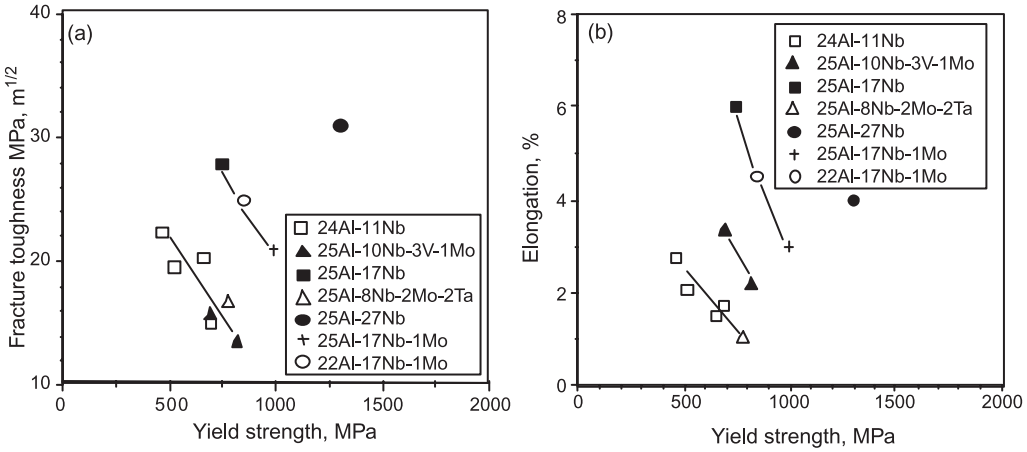

Figure 5. The evolution of strength, ductility and toughness with increasing Nb content in Ti_3Al–Nb and Ti_2AlNb alloys. **(a)** Fracture toughness as a function of yield strength in alloys of different Nb content **(b)** Elongation as a function of yield strength in alloys of different Nb content (Banerjee 1994).

toughness and creep, and then, recent research results (Carisey *et al* 2000) that are derived from this knowledge base.

3.2 *Microstructure, composition, strength, ductility and toughness*

The role of the *bcc* (B2) phase in defining strength, ductility and toughness is crucial in the development of optimized property levels. Figure 7 schematically indicates the principles involved. The B2 phase deforms by localized and heterogeneous, ⟨111⟩ slip. It fractures by cleavage when its grain size is large, and by ductile failure in ternary Nb-containing alloys when its grain size is small. The Ti_3Al phase fractures by cleavage, and deforms with less than five independent slip systems by $\langle 1\ 1\ \bar{2}\ 0\rangle$ slip on prismatic, $\{1\ 0\ \bar{1}\ 0\}$, and basal, (0001), planes. The B2 phase controls the fracture process in two distinct ways. If it films the Ti_3Al phase completely, onset of cleavage crack nucleation in Ti_3Al is delayed because it can relieve incompatibility stresses at Ti_3Al /B2 interfaces through its more isotropic deformation behaviour. In addition, when the thickness of the B2 phase between Ti_3Al particles is large enough, it can blunt cleavage cracks formed in the Ti_3Al phase.

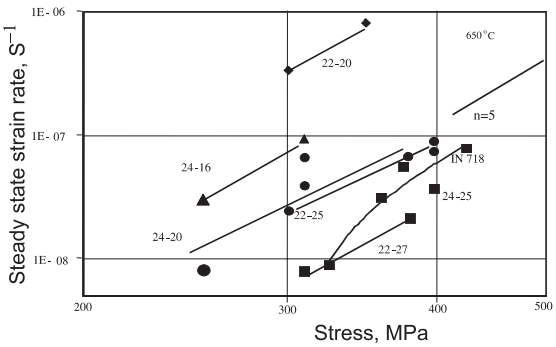

Figure 6. The effect of Al and Nb content on steady state creep in Ti2AlNb base alloys.

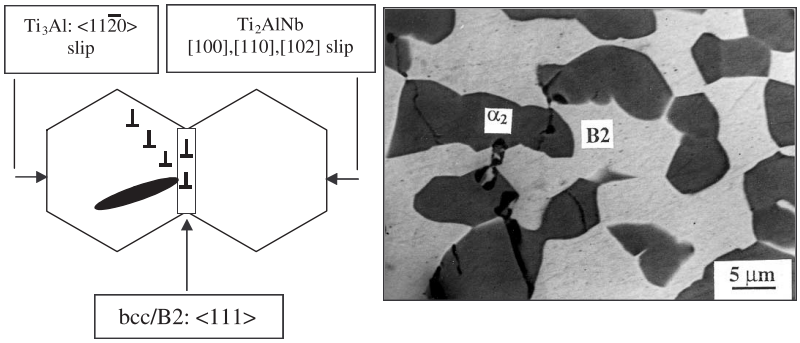

Figure 7. A schematic illustration of crack initiation and blunting, along with operative slip systems in *bcc* /B2, Ti_3Al , and Ti_2AlNb base alloys. The micrograph shows cleavage cracks in Ti_3Al blunted at the B2 phase.

The ductility rises sharply when the second effect is operative. Higher ductility or toughness is obtained when the Ti_2AlNb phase is present instead of Ti_3Al (Kamat *et al* 1998). Though the Ti_2AlNb phase also fails by cleavage, additional slip systems based on $c + a/2$ slip are observed in its deformation (Banerjee 1995; Nandy & Banerjee 1997). The value of its Poisson's ratio is also close to that found in metals (unlike the Poisson's ratio in Ti_3Al) (Chu 1997). The effect of the B2 phase content on strength, and ductility of alloys in this system is shown in figure 8. In view of the well-known effects of grain size on cleavage fracture stress in metals and alloys, it is also clear that the size of Ti_3Al or Ti_2AlNb particles in the structure must be restricted. The aluminum content of the B2 phase affects its mechanical behaviour significantly. At high Al contents (> 25 at%Al), the B2 phase exhibits a substantially greater tendency to brittle fracture. The strength of the B2 phase is higher than that of the Ti_3Al or Ti_2AlNb phases when its Al content is greater than about 20%, but drops with decreasing Al content (Kamat *et al* 1998; Boehlert 1997).

We summarize as follows: Alloys of the ternary Ti–Al–Nb contains the Ti_2AlNb or Ti_3Al and the B2 phases comprise a microstructural system in which the crack initiation occurs by

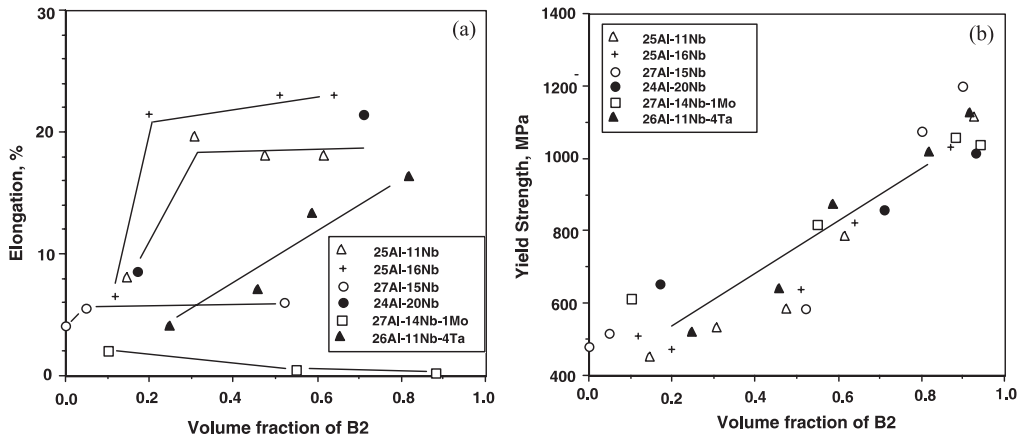

Figure 8. The effect of B2 volume fraction on the **(a)** elongation and **(b)** yield strength of Ti_3Al and Ti_2AlNb base alloys (Banerjee *et al* 1993).

cleavage of the Ti_3Al or Ti_2AlNb phase, and final fracture occurs by the linkage of these cracks through the B2 phase. The latter is ductile when its grain size and/or Al content is controlled below critical values. This process of fracture implies that a microstructure consisting of a fine distribution of the brittle phase completely enveloped by the relatively more ductile phase favour increased ductility and toughness. As shown in figure 8, fracture resistance can rise very substantially at high volume fractions of the B2 phase.

3.3 *Microstructure, composition and creep*

The creep strength of a relatively coarse two-phase system can be represented by a weighted fraction of the creep strengths of the individual phases. No data on the creep or diffusion in the B2 phase of the Ti–Al–Nb system is currently available. We expect that the creep resistance of the Ti_3Al and Ti_2AlNb phase will be substantially superior to that of the B2 phase, even though the latter is ordered. NiAl, for example, is weaker in creep than the Ni_3Al phase. Therefore, alloy design efforts have been directed towards structures with volume fractions of the Ti_2AlNb phase exceeding 95% to provide creep strength, but with adequate ductility and toughness. Within this framework, it has been established that the shape and size of the Ti_3Al or Ti_2AlNb phase significantly influences creep resistance. Lath-shaped particles offer better creep resistance than equiaxed particles (figure 9). Refining the lath size improves creep strength to a point beyond which resistance to creep again decreases. These results have been understood on the basis of two operative creep mechanisms, climb-controlled dislocation creep and diffusional creep, the latter providing substantial contributions to the total creep strain in steady-state creep when the equiaxed particles are present or when the lath size is extremely fine (Mishra *et al* 1996). Strong compositional effects are observed for a given microstructure. Creep resistance improves with increasing Al and Nb, with the Al effects being particularly strong Si additions are also beneficial, as in titanium alloys (Kerry 1992; Sagar *et al* 1995).

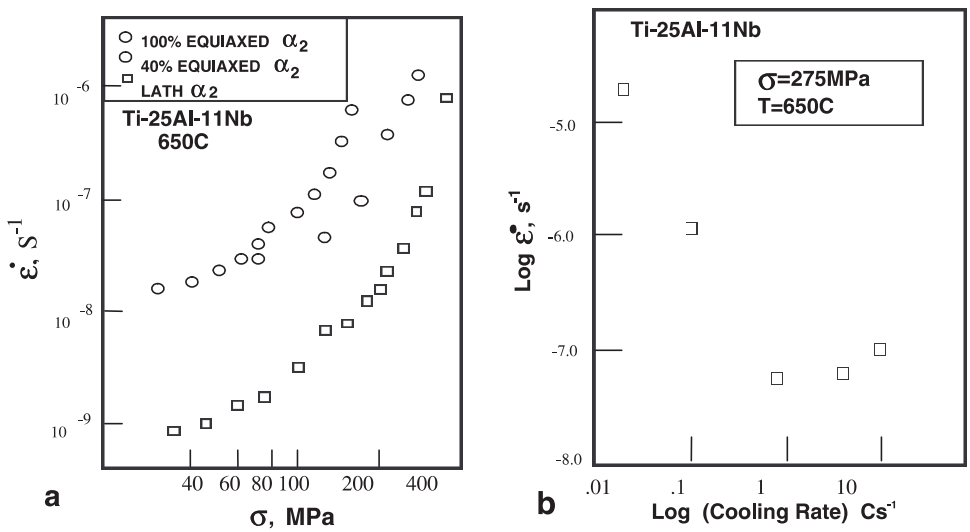

Figure 9. The creep of Ti_3Al–Nb phase alloys; **(a)** the effect of equiaxed Ti_3Al volume fraction on steady state creep; **(b)** the effect of cooling rate after solution treatment in the *bcc* phase region on steady state creep (Banerjee *et al* 1993).

3.4 *Enhanced ductility, toughness and creep*

Figure 10 shows a typical ternary, vertical section of the composition range of interest that forms a guide in our discussion on designed microstructures for superior combinations of properties. A given alloy composition solidifies into the *bcc* phase field and then passes through the $Ti_3Al + B2$, $Ti_3Al + Ti_2AlNb + B2$, and finally $Ti_2AlNb + B2$ phase fields on cooling. The *bcc* phase orders to the B2 phase, usually below 1200°C, but can disorder again if compositional equilibrium is reached at very low temperatures where Al content of the *bcc* phase is very low, a feature not apparent in the vertical section.

Processing followed by heat-treatment (solution treatment) in the single-phase *bcc* region (figure 11 – sequence A) results in recrystallized, coarse-grained *bcc* phase (since grain growth occurs very rapidly at these temperatures). The grain size is typically several hundred microns. Cooling from the *bcc* phase field results in the precipitation of lath structures of the Ti_3Al and the Ti_2AlNb phases. The formation of the former can be avoided at high enough cooling rates. The lath size decreases with increasing cooling rate, and the retained *bcc* /B2 phase is left behind as films between the laths. Whether these films are interconnected in the structure depends upon the residual volume fraction. Aging stabilizes the microstructure in a temperature range spanning potential service temperatures of the material.

Forging below the *bcc* transus offers the option of *bcc* grain size control, through the presence of a second phase, either Ti_3Al or Ti_2AlNb . The Ti_3Al and Ti_2AlNb phases also globularize by recrystallization to an equiaxed shape during the forging, if the deformation is adequate. The volume fraction of the equiaxed phase is determined by both the processing temperature and the heat-treatment (solution treatment) in the two-phase region (figure 11 – sequence B). Subsequent heat-treatment paths, such as cooling rates from solution-

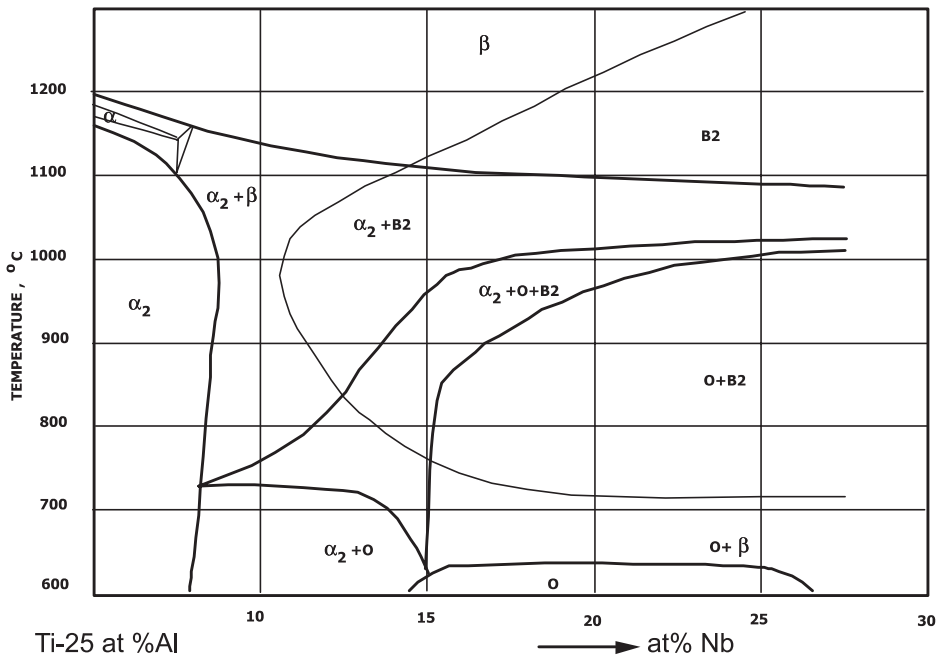

Figure 10. The vertical section at Ti–25 at·% Al in the Ti–Al–Nb system (Gogia *et al* 1998).

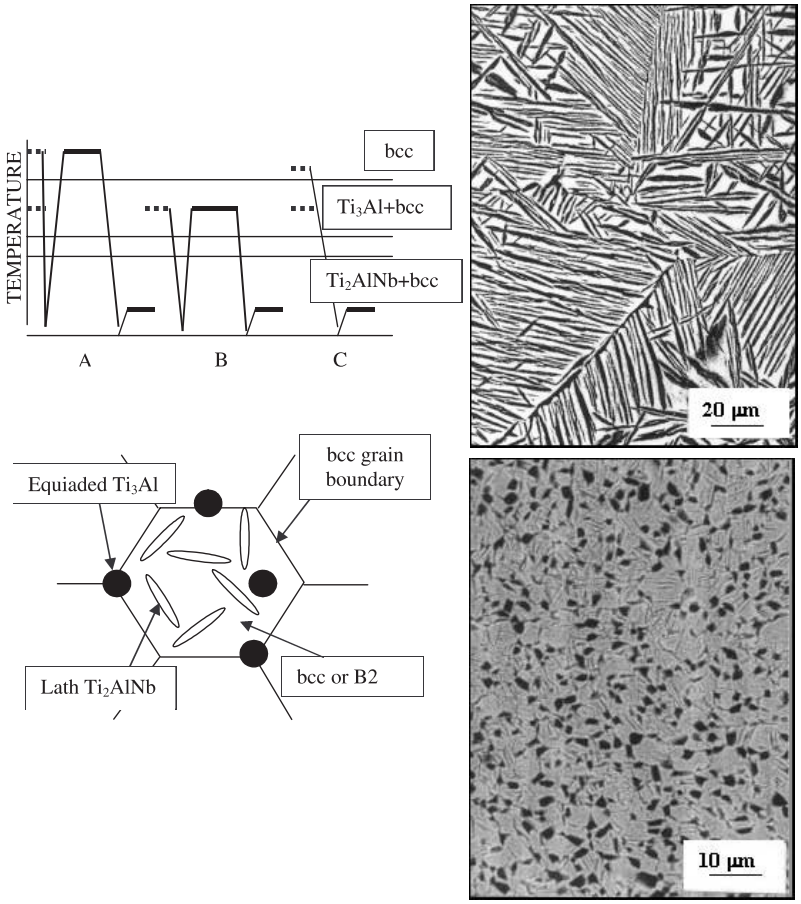

Figure 11. Processing sequences in Ti_2AlNb base alloys along with a schematic description of various microstructural parameters. The dashed lines indicate hot working sequences. Two typical microstructural variants are also shown.

treatment and the aging temperature and time, determine the scale of the lath structure that forms, as well as the final volume fraction of the residual B2 or *bcc* phase and its composition.

The prior *bcc* grain size (that is the size of the *bcc* grains established by solution treatment, within which precipitation of the Ti_3Al or Ti_2AlNb phase occurs on subsequent cooling or aging) is determined by whether particles of Ti_3Al or Ti_2AlNb are present or not during processing, and whether recrystallization occurs during processing and subsequent heat-treatment. In the range of Nb compositions relevant to the Ti_2AlNb alloys, it has been found that the recrystallization window occurs above the transus to the bcc phase field for simple processing sequences. In Nb lean alloys (up to about 15 at%Nb), recrystallization occurs into the two-phase field, so that the second phase particles can be effectively used to control prior *bcc* grain size during solution treatment. An alternative thermomechanical path is to directly age the material processed in the single-phase bcc region or in the two-phase region. A fine recrystallized or unrecrystallized prior *bcc* grain size, with a very fine intragranular precipitate structure may result (figure 11 – sequence C).

The role of the prior *bcc* grain size on mechanical behaviour has not been discussed in the preceding sections, where we focused on basic mechanisms governing fracture and creep. We have not found any effect of this microstructure parameter on steady-state creep. This is because creep is primarily controlled by the size and shape of the Ti_2AlNb or Ti_3Al phases and the volume fraction of the bcc phase. On the other hand, the prior *bcc* grain size does affect tensile fracture in the situation where the matrix is strengthened to very high levels. Under these conditions, fracture initiates at these grain boundaries and an intergranular, low ductility fracture mode is observed (Koss *et al* 1990). Such a low ductility fracture mode can be avoided if the prior *bcc* grain size can be substantially refined.

The phase diagram of figure 10 also suggests that the *bcc* phase is not available for ductilization at temperatures below about 600°C in the ternary alloys. Since this class of high temperature alloys is expected to see long time exposure in the temperature range 550°–650°C in service, it is essential that the *bcc* phase be further stabilized over that possible in the ternary alloys to precise levels required for ductilization, without seriously impairing creep properties. A decrease in Al content may achieve this, but this would result in unacceptable losses in creep properties, which are already marginal. It has been found that Mo, a strong *bcc* stabilizer, also confers high temperature strength. The level of Mo additions must be carefully optimized since it also embrittles the bcc phase. This understanding of processing and composition effects has been used to develop ternary and multicomponent alloys of this class (Carisey *et al* 2000), and some results from this research are shown in figure 12. The remarkable improvement in strength at ambient and high temperatures obtained by complex alloying is apparent, and the specific strength of these alloys is superior to that of the nickel-base alloy, IN 718, commonly used in aeroengine applications in the temperature range 550°–700°C. The significant effect of different processing and heat treatment sequences on the properties for a given composition is also quite apparent. Application of the principles of microstructural and compositional optimization described above results in an excellent combination of strength, ductility and creep properties in the multicomponent alloy with the thermomechanical process labeled B in the figure.

4. Intermetallics based on the Fe_3Al-C system

4.1 *Background*

The excellent corrosion resistance of Fe_3Al has been known since the 1930s. The mechanical behaviour of Fe_3Al was studied through the 1950s and 1960s, and it was recognized that the ductility of this intermetallic compound drops sharply when the Al content approaches the stoichiometric composition. It was also recognized that its yield strength and creep is limited by the transition of DO_3 order to B2 order at approximately 550°C in the stoichiometric composition. The ductility of the intermetallic was shown to be dependent on the hydrogen content of the test environment, and it was established that Fe_3Al is intrinsically ductile. Additions of Cr and Zr (in the absence of carbon) were found to be beneficial in imparting ductility in normal test environments, while a variety of additions such as Nb and Mo were shown to enhance creep resistance. Some of these additions form the basis of Fe_3Al -base alloys developed at the Oak-Ridge National Laboratory. The melting of Fe_3Al alloys presents difficulties that arise from the interaction of Al in the alloy with moisture to form hydrogen-induced porosity. This can be avoided by vacuum induction melting or vacuum arc re-melting, but clearly cost is a serious consideration relative to stainless steels. The history of development of Fe_3Al alloys has been recently reviewed (McKamey *et al* 1991; Sikka 1997; Stoloff 1998).

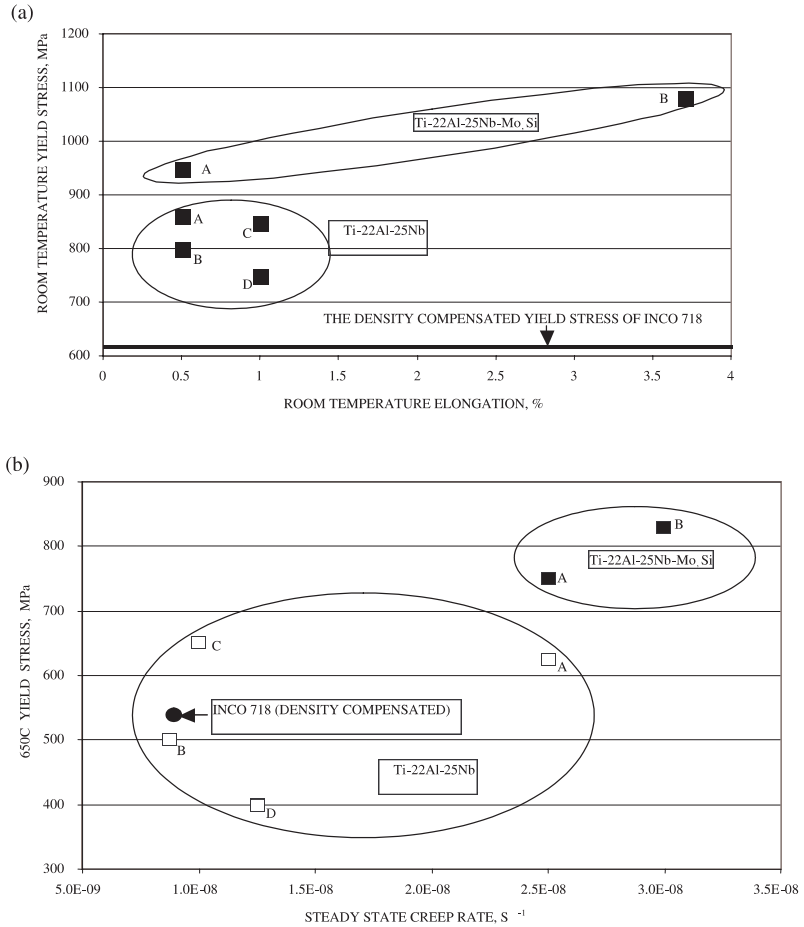

Figure 12. The effect of alloy composition and processing on the tensile and creep properties in the orthorhombic aluminides.

4.2 *The microstructure of Fe_3Al–$Fe_3AlC_{0{\cdot}5}$ alloys*

In our laboratory we investigated the effect of carbon additions to Fe_3Al base alloys. Melting sound, porosity free Fe_3Al alloys was accomplished by cost-effective techniques of using a special flux cover in air induction melting, or electro slag re-melting (ESR) of air-melted ingots (Baligidad *et al* 1996). These melting techniques will not be described in detail here, but are obviously crucial in cost control in the processing of Fe_3Al base alloys. A ternary section of the Fe–Al–C section at 1 wt %C is shown in figure 13. The phase diagram suggests that α-iron solidifies from the melt phase at the Fe_3Al composition. Subsequently, the alloy passes through a three-phase $\alpha + L + Fe_3AlC_{0{\cdot}5}$ into the two-phase $Fe_3Al + Fe_3AlC_{0{\cdot}5}$ phase field. The $Fe_3AlC_{0{\cdot}5}$ phase has a perovskite structure. Figure 14 shows the effect of carbon content on the as-cast microstructure of ESR melted ingots of Fe_3Al . No $Fe_3AlC_{0{\cdot}5}$ phase is observed in the 0·01 wt% carbon alloy. Volume fraction of the $Fe_3AlC_{0{\cdot}5}$ phase increases with carbon content beyond this level. The Fe_3Al phase appears as a precipitate within Fe_3Al grains up to carbon contents of 0·5 wt %C, and as an interdendritic phase at the carbon level of 1·1 wt%. This suggests that the three-phase field, $\alpha + Fe_3Al + Fe_3AlC_{0{\cdot}5}$, is very narrow

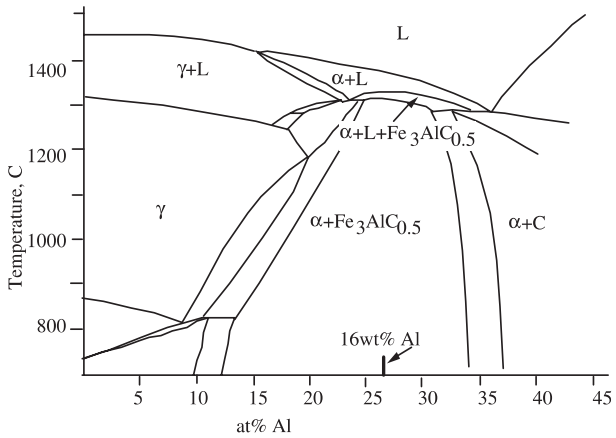

Figure 13. The vertical section at Fe–1·1 wt% C in the Fe–Al–C system (Palm & Inden 1995).

up to a carbon level of 0·5 wt%, such that the alloys are able to solidify completely as α-iron at the operative solidification rates before $Fe_3AlC_{0\cdot5}$ phase formation occurs. Graphite is present in the alloy containing 1·8 wt% carbon, showing that two-phase $Fe_3Al + Fe_3AlC_{0\cdot5}$ region ends just beyond 1·1 wt% carbon.

4.3 *Room temperature tensile properties of Fe_3Al–$Fe_3AlC_{0\cdot5}$ alloys*

Figure 15 shows the tensile properties of as-cast air induction and ESR Fe_3Al –$Fe_3AlC_{0\cdot5}$ alloys at room temperature as a function of carbon content (Baligidad *et al* 1996). The alloys with low carbon content fail without any ductility. Microcracks are observed in these alloys (figure 14a). These may be responsible for the premature failure of these samples. Measurable plasticity is observed in the higher carbon alloys, and in these the yield strength also increases with carbon content. The microhardness of the $Fe_3AlC_{0\cdot5}$ phase (590 HV) is significantly higher than that of the Fe_3Al phase (360 HV), and the experimentally measured bulk hardness follows the rule of mixtures (Baligidad *et al* 1998). These results are unusual in that the presence of the harder, and possibly more brittle, $Fe_3AlC_{0\cdot5}$ phase leads to expected strengthening but also retains plasticity in the material. The failure mechanisms in the tensile mode were further explored through the microstructural examination of longitudinal sections of tensile samples to identify failure initiation sites. Figure 16 shows the results for the high carbon material with a substantial volume fraction of the carbide phase. The fracture surface shows evidence of both cleavage and plastic tearing. While cleavage cracks are observed in the carbide phase, these terminate at the carbide boundaries and do not lead to fracture of the matrix. The dominant initiation mode appears to be that of void nucleation at the interfaces between the carbide and the intermetallic matrix, especially in locations where the volume fraction of the intermetallic phase is low. Final fracture occurs by cleavage of the remaining intermetallic matrix ligaments. It is clear that the presence of the carbide has enhanced the fracture stress of the matrix such that void nucleation of the carbide/intermetallic interfaces precedes cleavage of the matrix. It is possible that the carbide acts as traps for hydrogen, which is believed to be the cause for the embrittlement of the matrix. However, cleavage of the $Fe_3AlC_{0\cdot5}$ particles limits the ductility.

The tensile properties shown in figure 15 are for the as-cast structures of ESR melted ingots. The grain size of the matrix is very large, and of the order of millimetres. The matrix grain size can be refined by forging or rolling (Baligidad *et al* 1996), but this offers no improvements in ductility, reinforcing the conclusion that failure is controlled by void nucleation at

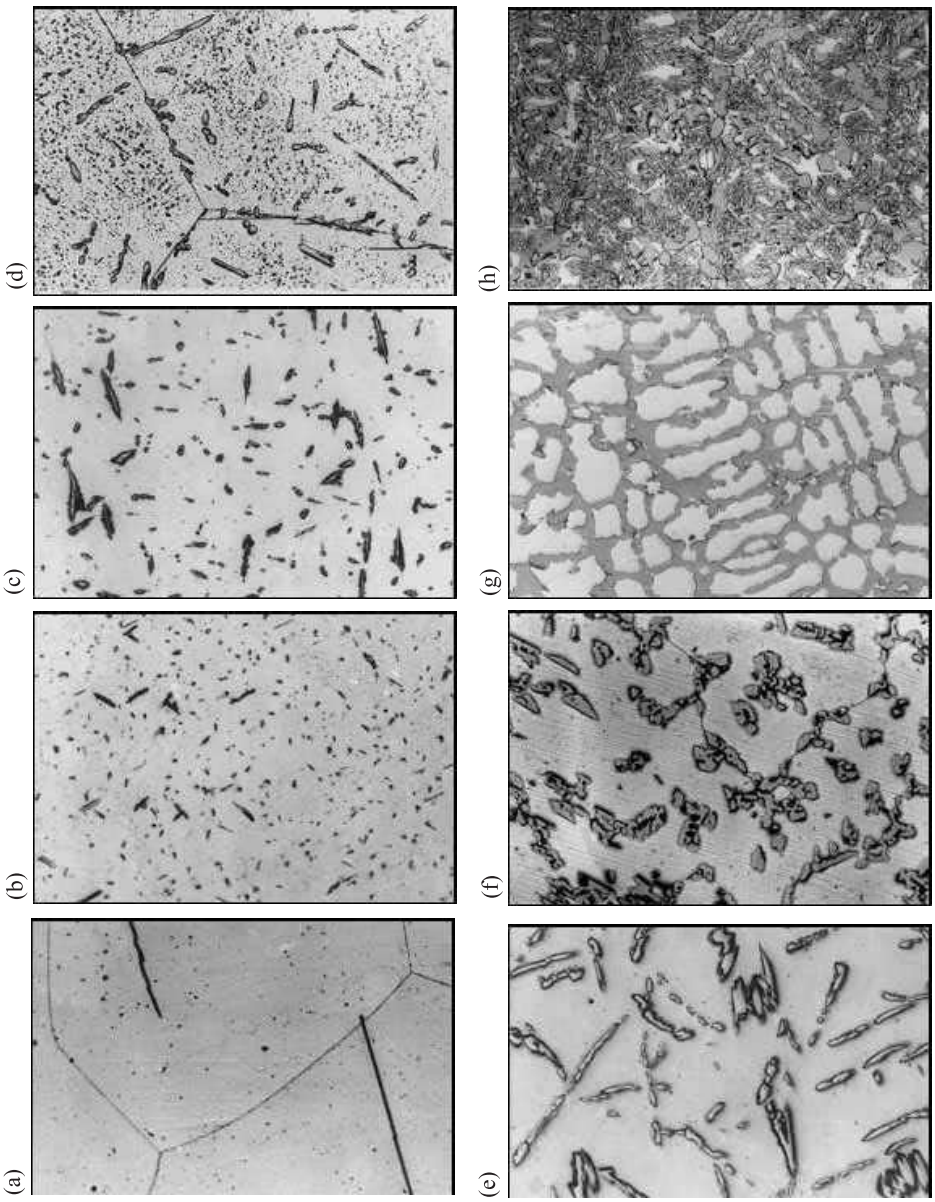

Figure 14. The effect of C content on as-cast microstructures of Fe–16 wt·% Al alloys as a function of carbon content; **(a)** 0·01 wt·% C, **(b)** 0·03 wt·% C, **(c)** 0·07 wt·% C, **(d)** 0·14 wt·% C, **(e)** 0·27 wt·% C, **(f)** 0·5 wt·% C, **(g)** 1·1 wt·% C, **(h)** 1·8 wt·% C.

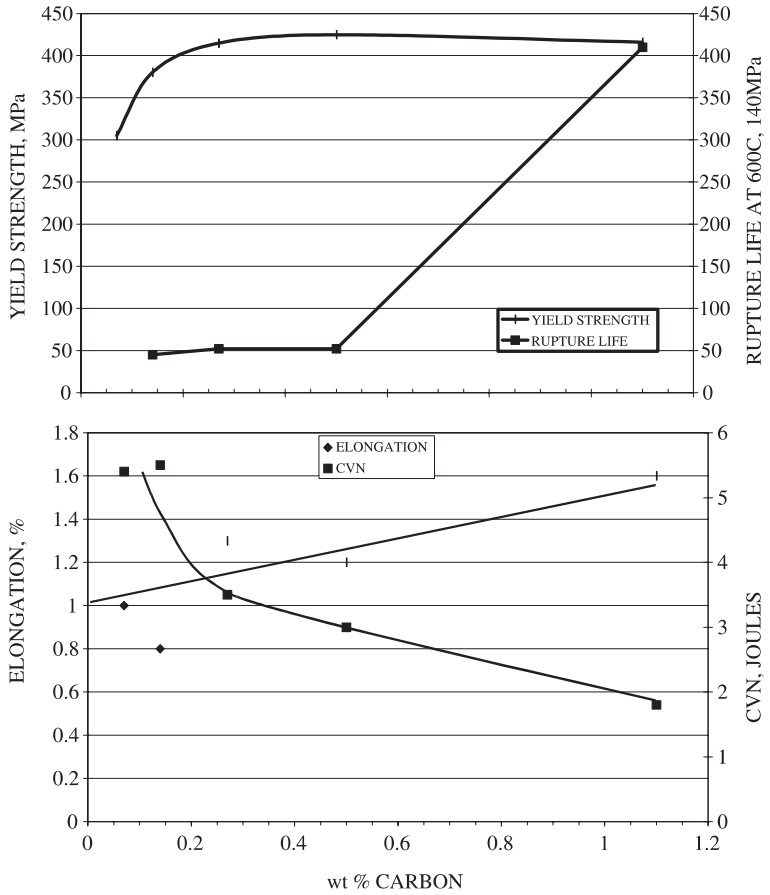

Figure 15. Tensile and creep properties of Fe–16 wt% Al alloys as a function of carbon content.

carbide/intermetallic interfaces. It must be noted that the plasticity achieved by the presence of the carbide does not translate to improved impact resistance at high strain rates with charpy V-notch values of around 3–5 joules obtained irrespective of the carbon content. It is also recognized that the ductility achieved is lower than that obtained in Fe_3Al alloys with other beneficial alloying additions and carefully processed to achieve unrecrystallised, elongated grain structures lying parallel to the surfaces of tensile samples. Nevertheless, the achievement of reasonable engineering plasticity in as-cast structures with alloying elements as inexpensive as Al and C represents a significant breakthrough in this class of alloys.

4.4 *High temperature properties of Fe_3Al–$Fe_3AlC_{0{\cdot}5}$ alloys*

Figure 17 shows the effect of temperature on the tensile properties of the high carbon alloy at different Al levels (Baligidad *et al* 1997). A significant strengthening is present at intermediate temperatures, and the yield strength drops above 600°C. The ORNL wrought alloy at the same aluminum level shows no anomalous strengthening. The yield strength is substantially higher than that of stainless steel.

The creep properties have been shown as a function of carbon content in figure 15. As in the case of tensile properties, a significant effect of carbide volume fraction is observed.

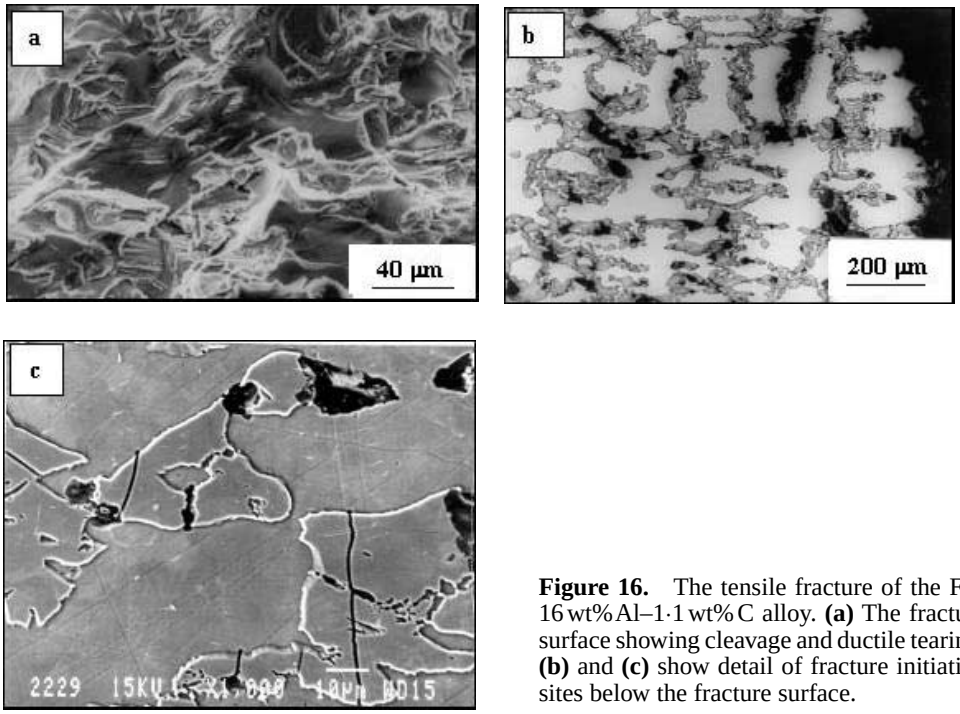

Figure 16. The tensile fracture of the Fe–16 wt% Al–1·1 wt% C alloy. **(a)** The fracture surface showing cleavage and ductile tearing; **(b)** and **(c)** show detail of fracture initiation sites below the fracture surface.

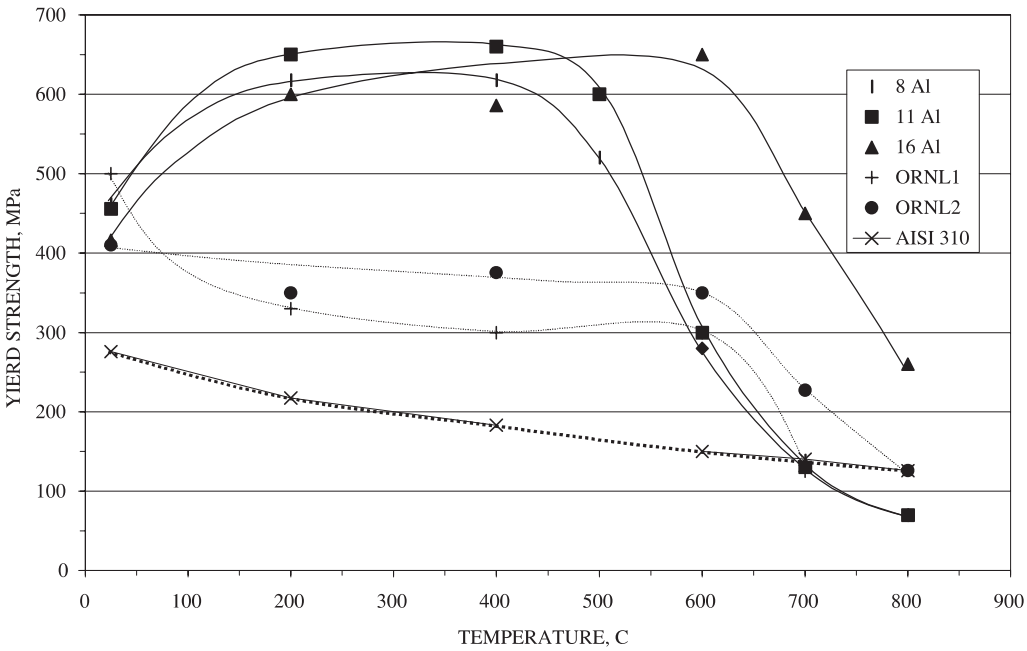

Figure 17. Yield stress of the Fe_3Al –C alloys containing 1·1 wt% C as a function of temperature in relation to stainless steel, and vacuum melted and wrought Fe_3Al base alloys developed at ORNL, USA.

The creep properties of the $Fe_3AlC_{0\cdot5}$ phase are not available. It is likely that the carbide is significantly stronger in creep, and that the creep strength of the coarse two-phase structure is determined by a simple volume fraction weighted average of the properties of the constituent phases. While the tensile strength of the Fe_3Al –$Fe_3AlC_{0\cdot5}$ alloys are much higher than that of stainless steel, the creep properties are substantially poorer though both constituent phases are ordered. The creep life of the as-cast Fe_3Al –$Fe_3AlC_{0\cdot5}$ alloy is better than that of the wrought Fe_3Al alloy developed at ORNL.

5. Summary

We have described the effect of second-phase additions and compositional effects on the microstructure and properties of intermetallics alloys based on Ti_2AlNb in the Ti–Al–Nb system and Fe_3Al in the Fe–Al–C system. In the former, the ductile *bcc* phase of titanium or its ordered B2 counterpart is used to confer ductility and toughness. This is achieved together with reasonable creep strength through the adjustment of Ti_2AlNb volume fraction, size and shape through appropriate thermomechanical processing. In the latter, the addition of large amounts of carbon to the Fe_3Al phase is shown to result in a coarse two-phase structure consisting of the Fe_3Al and $Fe_3AlC_{0\cdot5}$ phases. The presence of the latter leads to engineering plasticity in the system, possibly by ameliorating the well-known hydrogen effect. Concomitantly, the presence of the $Fe_3AlC_{0\cdot5}$ phase also leads to significant improvements in tensile and creep properties.

The financial support of the Defence Research and Development Organization of India for part of this work is acknowledged. Recent results on ternary and multicomponent Ti_2AlNb alloys were generated in collaborative programs between DMRL, SNECMA, Ecole Des Mines and Turbomeca. The authors also wish to acknowledge the numerous contributions of their colleagues at DMRL in the two research programmes described here, especially T K Nandy, K Muraleedharan, P K Sagar, R S Mishra, U Prakash and A Radhakrishna. We also express our gratitude to J L Strudel for many inspiring discussions.

References*

Baligidad R G, Prakash U, Radhakrishna A, Ramakrishna Rao V, Rao P K, Ballal N R 1996a *ISIJ Int.* 36: 1215
Baligidad R G, Prakash U, Ramakrishna Rao V, Rao P K, Ballal N B 1996b *ISIJ Int.* 36: 1448
Baligidad R G, Prakash U, Ramakrishna Rao V, Rao P K, Ballal N B 1996c *ISIJ Int.* 36: 1453
Baligidad R G, Prakash U, Radhakrishna A 1997 *Mater. Sci. Eng.* A231: 206
Baligidad R G, Radhakrishna A, Prakash U 1998 *Mater. Sci. Eng.* A257: 235
Banerjee D 1994 In *Intermetallic compounds – Principles and practise* (eds.) J Westbrook, R L Fleischer (New York: John Wiley and Sons) p 91
Banerjee D 1995 *Philos. Mag.* A72: 1559
Banerjee D 1997 *Prog. Mater. Sci.* 42: 135
Banerjee D, Gogia A K, Nandy T K, Joshi V A 1988 *Acta Metall.* 36: 871

*References in this list are not in journal format

Banerjee D, Gogia A K, Nandy T K, Muraleedharan K, Mishra R S 1993 In *Structural intermetallics* (eds) R Darolia, J J Lewandowski, C T Liu, P L Martin, D B Miracle, M V Nathal (Warrendale, PA: The Mater. Soc.) p 19

Blackburn M J, Smith M P 1978 Research to conduct exploratory and analytical investigations of alloys. AFML-TR-78-18, USA

Boehlert C J 1997 WL-TR-97-418, USA

Carisey T, Germann L, Strudel J L, Vikas Kumar S, Nandy T K, Gogia A K, Banerjee D, Franchet J M, Gedou J Y 2000 Research in progress. Ecole Des Mines, Paris, France, DMRL, India, Snecma, France

Chu F, Mitchell T E, Majumdar B, Miracle D, Nandy T K, Banerjee D 1997 *Intermetallics* 5: 147

Gogia A K, Nandy T K, Banerjee D, Carisey T, Strudel J L, Franchet J M 1998 *Intermetallics* 6: 74

Kamat S K, Gogia A K, Banerjee D 1998 *Acta Mater.* 46: 239

Kerry S 1992 DRA Tech. Report 92019, UK

Koss D A, Banerjee D, Lukasak D A, Gogia A K 1990 In *High temperature aluminides and intermetallics* (eds.) S H Whang, C T Liu, D P Pope, J O Steigler (Warrendale, PA: The Mater. Soc.) p 175

McAndrew J P, Simcoe C R 1961 Development of a Ti–Al–Cb alloy for use at 1200F-1800F. ASD-TR-61-466, USA

McKamey C G, DeVan J H, Tortorelli P F, Sikka V K 1991 *J. Mater. Res.* 6: 1779

Mishra R S, Nandy T K, Sagar P K, Gogia A K, Banerjee D 1996 *Trans. Indian Inst. Met.* 49: 331

Nandy T K, Banerjee D 1997 In *Structural intermetallics* (eds.) M V Nathal, R Darolia, C T Liu, P L Martin, D B Miracle, D B Miracle, R Wagner, M Yamaguchi (Warrendale, PA: The Mater. Soc.) p 777

Palm M, Inden G 1995 *Intermetallics* 3: 493

Rowe R G 1991 *US Patent* 5 032 357, USA

Sagar P K, Nandy T K, Gogia A K, Muraleedharan K, Banerjee D 1995 *Mater. Sci. Eng.* 192/193: 799

Sikka V K 1997 *Int. Symp. on nickel and iron aluminides: Processing, properties, and applications* (Materials Park, OH: ASM Int.) p. 361

Stoloff N S 1998 *Mater. Sci. Eng.* A258: 1